UC San Diego
UC San Diego Previously Published Works

Title

Qualitative and Quantitative Ultrashort Echo Time Imaging of Musculoskeletal Tissues.

Permalink

https://escholarship.org/uc/item/4mr176hv

Journal

Seminars in musculoskeletal radiology, 19(4)

ISSN

1089-7860

Authors

Chang, Eric Y
Du, Jiang
Bae, Won C
et al.

Publication Date

2015-09-01

DOI

10.1055/s-0035-1563733

Copyright Information

Peer reviewed

Qualitative and Quantitative Ultrashort Echo Time Imaging of Musculoskeletal Tissues

Eric Y. Chang, MD[1,2]   Jiang Du, PhD[2]   Won C. Bae, PhD[2]   Christine B. Chung, MD[1,2]

[1] Department of Radiology, VA San Diego Healthcare System, San Diego, California
[2] Department of Radiology, University of California, San Diego Medical Center, San Diego, California

Address for correspondence Eric Y. Chang, MD, Department of Radiology, VA San Diego Healthcare System, 3350 La Jolla Village Drive, MC 114, San Diego, CA 92161 (e-mail: ericchangmd@gmail.com).

Abstract

Keywords

► magnetic resonance imaging
► ultrashort echo time
► UTE
► short T2/T2*
► musculoskeletal

Ultrashort echo time (UTE) sequences represent a group of clinically compatible techniques that are capable of using echo times < 1 ms. With these techniques, direct imaging of short T2/T2* tissues or tissue components can now be performed. Continuing modifications to the UTE techniques have allowed for faster and more robust sequences now comparable with conventional clinical sequences. UTE also allows for morphological imaging and quantitative evaluation in a manner not previously possible with conventional imaging sequences utilizing much longer echo times. Numerous potential clinical applications have emerged that are discussed in this review article.

Since the earliest years of clinical MR imaging, the primary focus has been on tissues with long T2 relaxation.[1,2] Included in this group are tissues that normally demonstrate a relatively long T2 such as the brain and liver. It has long been recognized certain tissues with short mean T2 components typically lack detectable signal using conventional sequences, such as normal cortical bone and tendon.[3] These tissues can only be visualized when affected by advanced pathology, causing an increase in water and water mobility, such as when fluid is located in the gap of a torn tendon. However, there is no opportunity to diagnose disease in earlier states, and contrast manipulation of tissue constituents or the evaluation of contrast enhancement is impossible. Furthermore, quantitative measurements of tissue (including T1, T2, T2*, T1ρ, proton density [PD], and magnetization transfer) are not feasible.

In more recent years, a group of clinically compatible sequences has emerged that can image tissues with very short transverse relaxation times, together referred to as the ultrashort echo time (UTE) group of sequences.[4] Common to this group is a reduction of echo time (TE), which allows for the detection of a short T2/T2* signal. With detectable signal from short T2/T2* tissues, both morphological and quantitative evaluation become possible. This promises to revolution-ize musculoskeletal imaging. Rather than relying on pathologic increases in T2 to visualize structures such as bone, tendons, ligaments, and menisci, we now have the opportunity to visualize the tissue directly and evaluate tissue components and properties selectively.

This article reviews the UTE group of sequences in three parts. First, we review the UTE sequence and subsequent modifications used to improve coverage, speed, or contrast. Second, we review morphological and quantitative imaging techniques that have emerged using UTE sequences. Finally, we discuss potential the clinical applications of UTE sequences including highlighting anatomy that has not been seen using conventional clinical sequences.

Techniques

The slice-selective UTE sequence was first described in 1989 by Pauly et al.[5] The TE is limited only by the time required to turn off the radiofrequency (RF) excitation and to enable the receiver. K-space is filled with a radial trajectory, with the acquisition starting at the center. By beginning at the center of k-space, multiple delays can be eliminated including those associated with the phase-encode gradient, dephasing gradient, and first half of the readout gradient.[5,6] Data sampling
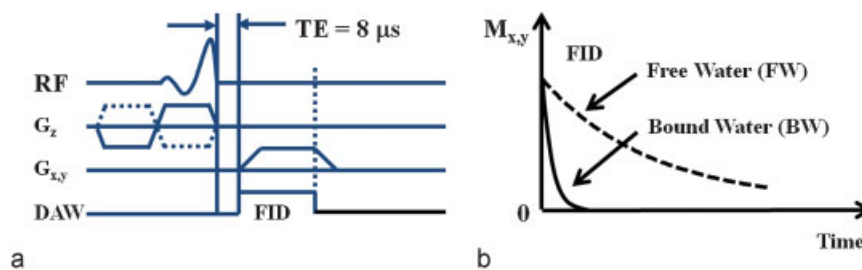
Fig. 1 (a) The two-dimensional ultrashort echo time pulse sequence. (b) Magnetization diagram. Two-dimensional imaging utilizes slice selection performed with two half excitations: the first with a positive gradient and the second with a negative gradient, combining to add as a single complete excitation pulse. Data acquisition begins while the readout gradient is being ramped. DAW, digital acquisition window; FID, free induction decay; RF, radiofrequency.

occurs as the acquisition gradient is being ramped up and continues through the plateau (►**Fig. 1**). Two-dimensional (2D) imaging utilizes slice selection, performed with two half excitations: the first with a positive gradient and the second with a negative gradient, combining to add as a single complete excitation pulse. Three-dimensional (3D) imaging can be performed with a nonselective short rectangular pulse and 3D radial acquisition.[6] By using appropriate coils and prescription of the field of view, aliasing can be avoided. After acquisition, the raw k-space data are mapped onto a grid and reconstructed by inverse Fourier transform.

UTE sequences suffer from relatively long acquisition times. With 2D UTE sequences, two TR periods per line of k-space are required (compared with one used in conventional 2D sequences), and a single radius of k-space is mapped (compared with a Cartesian line in conventional sequences). In addition, radial mapping is less effective than rectilinear (Cartesian) methods because there is tremendous oversampling of low frequencies and undersampling of high frequencies ($\pi/2$ times more TRs are required for the k-space periphery to satisfy the Nyquist criteria).[7] However, more advanced trajectories have been proposed to improve efficiency including spiral and cones projection methods for k-space filling.[8,9] Other sequences in the UTE family used on clinical scanners include the acquisition-weighted stack of spirals sequence[10] that uses selective excitation, variable-duration slice encoding, and mobile spiral readout to sample a cylindrical volume in k-space and the variable TE sequence[11] that uses Cartesian k-space sampling with asymmetric RF pulses, partial echoes, and ramp sampling. With UTE sequences, TEs as short as 8 µs (0.008 ms) have been achieved, although TE values ranging from 20 to 100 µs are more typical.

Another group of sequences does not switch off the readout gradients between successive TR intervals but only slightly adjusts them. Because encoding starts at full speed immediately at the time of excitation, a nominal TE of zero is achieved, hence the name zero TE (ZTE).[12,13] ZTE uses a nonselective hard pulse excitation followed by 3D center-out radial sampling. The RF pulse can also be a longer, frequency-modulated pulse with an interleaved transmit-receive operation, known as sweep imaging with Fourier transformation (SWIFT).[14] The finite RF transmit-receive switching times between excitation and reception lead to a spherical gap in the center of k-space. Multiple methods of addressing this problem have been proposed including acquisition oversampling and algebraic reconstruction in the ZTE technique[12] or filling with a Cartesian single-point imaging technique, known as pointwise encoding time reduction with radial acquisition (PETRA).[15] ZTE techniques have potential for imaging spins with extremely short T2/T2*s, such as collagen protons, which may not be directly detectable with UTE sequences.

Morphological Evaluation

UTE sequences detect signal from tissues with both long and short/ultrashort mean transverse relaxation times. However, signal-to-noise and contrast-to-noise ratios are not synonymous, and there can be insufficient contrast between structures for optimal morphological evaluation when using UTE sequences. The simplest technique for selective visualization of short T2/T2* components is with image subtraction between a UTE image (which detects long and short T2* components) and an image with a longer TE (which detects longer T2* components) (►**Fig. 2**). Variable weighting of the subtraction images can provide improved contrast of tendons, cartilage, bone, and menisci.[16]

Selective visualization of short T2/T2* components can also be achieved with the use of preparation pulses including saturation or inversion pulses. Saturation of long T2* components can be achieved with a long RF pulse followed by a crusher gradient and subsequent UTE imaging.[17,18] This technique relies on the fact that the short T2* components experience significant transverse relaxation during the long RF pulse and cannot be saturated. Thus significant longitudinal magnetization exists after the long saturation pulse and provides the short T2* signal and contrast. The use of two consecutive saturation pulses and spoilers can be used for combined water and fat suppression, known as water- and fat-suppressed projection imaging (WASPI).[17] Off-resonance saturation with UTE acquisition and subtraction can provide high contrast images of short T2* components.[19] This technique exploits the broad spectral linewidths (several kilohertz) that short T2* components demonstrate. An RF pulse placed at a frequency far from the narrow linewidths of long T2 water and fat is expected to selectively suppress the short T2* components, either through direct saturation,[20] cross-

Fig. 2 Coronal images of a right knee of a patient using (**a**) three-dimensional ultrashort echo time (3D-UTE)-Cones technique with 0.03 ms TE and (**b**) subtraction technique (0.03 ms minus 4.4 ms TEs). Subtraction images show improved contrast with selective visualization of short T2 components including the calcified layer of cartilage (arrows) and tibial collateral ligament (black arrow). Note hypointense superficial layer of cartilage on subtraction image (dashed arrows), indicating this tissue contains predominantly long T2 components. Dual echo-UTE-Cones acquisition time was ∼ 6 minutes.

relaxation between collagen protons and protons in bound water[21] or chemical exchange between bound and free water.[22] Subtraction of the two UTE images, acquired with and without the off-resonance preparation pulse, will highlight the short $T2^*$ components.

Short $T2^*$ components can also be selectively imaged using inversion recovery (IR) pulses. With single IR-UTE, a relatively long single adiabatic inversion recovery pulse (8.6 ms in duration) is used to invert the longitudinal magnetization of long $T2^*$ water.[8,23,24] UTE data acquisitions are then begun at an inversion time (TI) designed to allow the inverted longitudinal magnetization of free water to be close to the null point[8] (►**Figs. 3a, b**). Magnetization of fat is also inverted along with free water, and > 80% nulling of the signal from both fat and long-$T2^*$ components can be achieved with a single inversion pulse. Alternatively, two inversion pulses can be used, such as with the double IR-UTE technique, allowing more complete nulling of both fat and long $T2^*$ water components[25,26] (►**Figs. 3c, d**). Inversion-based approaches are less signal-to-noise efficient compared with saturation-based approaches but are much less sensitive to B_0 and B_1 inhomogeneities.

Differences in phase between tissues and tissue components can also be used for morphological evaluation. During the RF pulse and readout periods of the UTE sequence, differences in phase manifest and can be used as a contrast mechanism.[27] In some instances, phase images may provide more contrast between structures compared with magnitude images,[18] and the combination of the two can yield very high contrast susceptibility-weighted images.[28]

Quantitative Evaluation

Using the UTE techniques, quantitative measurements of nuclear magnetic resonance relaxation times can also be performed. One of the most frequently used techniques is measurement of transverse decay times. Using a constant repetition time (TR) and variable TE, beginning with an ultrashort TE, $T2^*$ can be quantified. Because the UTE technique is a gradient-echo type sequence without a refocusing pulse, $T2^*$ rather than T2 is measured, and relaxation time is dependent on spin-spin interaction, tissue hydration, and susceptibility effects.[29] However, the use of the UTE does not allow for much true T2 decay to occur,[30] and for fast relaxing components, $T2^*$ approaches T2.[6]

From signal intensity measurements generated from the multiple TE images, $T2^*$ can be fit using a monoexponential decay model or with a multiexponential decay model. A monoexponential (or single-component) model measures the mean transverse relaxation time within a voxel or region of interest. However, in actuality, all biological tissues are heterogeneous and contain a combination of tissue components. With the UTE technique, tissues of the musculoskeletal system can be divided into components with "short" and "long" relaxation times, representing
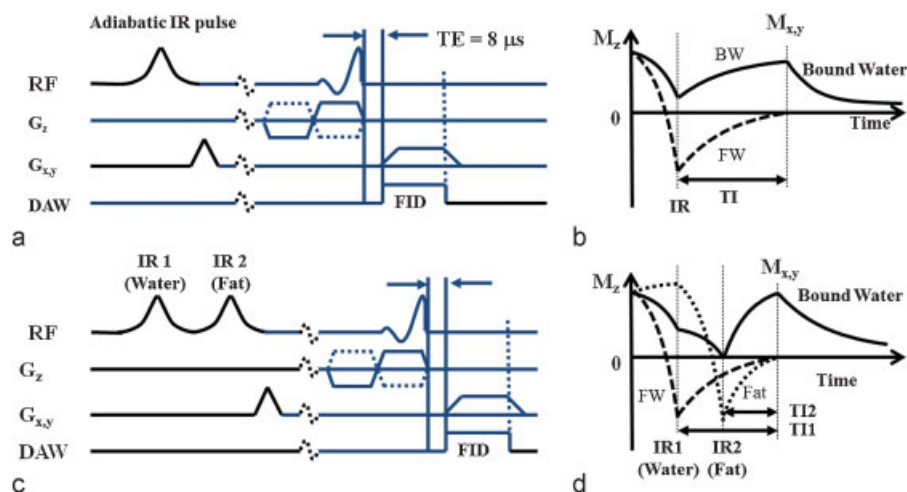
Fig. 3 The inversion recovery (IR) single ultrashort echo time (UTE) (**a**) and double IR-UTE pulse sequences (**c**) are shown with contrast mechanisms, (**b**) and (**d**), respectively. In single IR-UTE (a, b), a single adiabatic IR pulse is used to invert and null the free water magnetization. The bound water magnetization is not inverted and is detected using a UTE data acquisition. In double IR-UTE (c, d), two IR pulses are used to invert and null the longitudinal magnetization of long T2 water and fat, respectively. Recovered bound water signal is detected with a UTE data acquisition. BW, bound water; DAW, digital acquisition window; FID, free induction decay; FW, free water; RF, radiofrequency.

water bound to macromolecules (such as collagen and proteoglycan/glycosaminoglycan [GAG]) and free water, respectively.[31]

Models that contain more than two components have not been used routinely on clinical imaging systems. In particular, multiexponential T2* analyses are very sensitive to spatial resolution, image signal-to-noise ratio, the number and spacing of echoes, the number of fitting components, and the differences between T2* values of individual components.[32] Much of the data on the total number and relaxation times of measureable components comes from studies using high-performance spectroscopic systems and Carr-Purcell-Meiboom-Gill (CPMG) sequences that contain refocusing pulses and therefore measure T2. Although measurements made with the UTE sequence will incorporate susceptibility effects resulting in T2* values that are shorter than T2, it is assumed that the number and relationship between components is similar between measurements made with CPMG sequences on spectroscopic systems and measurements made with UTE sequences on clinical MRI systems. With regard to the reproducibility of T2* quantification, similar results have been obtained when comparing 2D-UTE, 3D-UTE, and 3D-UTE-Cones sequences.[33]

T2* measurements are complicated by the magic angle effect.[34] It can cause a 10-fold difference in signal intensity[34] and significant variations in mono- and biexponential T2* measurements. For anisotropic tissues, Wang and Xia demonstrated that both the total number and component T2 relaxation times vary depending on orientation with respect to B_0.[35] Despite this, previous studies have shown that data from UTE sequences with bicomponent T2* analyses (specifically percentage of short and long components) is less sensitive to magic angle effects compared with monoexponential T2*.[36]

T1ρ has also been measured with the UTE sequence. In T1ρ imaging, a 90-degree pulse is delivered and a spin-lock pulse is applied. During the locking pulse, spin relaxation occurs via the time constant T1ρ. Thereafter, a − 90-degree pulse flips the magnetization back into the longitudinal plane, a crusher gradient spoils residual transverse magnetization, and the UTE sequence is used for acquisition. Using various spin-lock times, T1ρ is quantified using either a mono- or multiexponential decay model.[37] Similar to T2, T1ρ as measured with the UTE technique has been shown to be strongly affected by the magic angle effect.[38]

Techniques that are less sensitive to magic angle effects include T1 relaxation and magnetization transfer (MT) techniques. T1 relaxation time depends on tissue water content as well as the macromolecular environment.[29] T1 quantification of short T2* tissues has been performed using saturation recovery[18,39] and variable flip angle[40] approaches combined with UTE acquisition, for 2D and 3D imaging, respectively. MT refers to transfer of longitudinal magnetization from the bound proton pool to the free proton pool. When combined with the UTE sequence, MT imaging can be performed on short T2 tissues. The UTE-MT sequence uses an off-resonance saturation pulse for MT preparation. The off-resonance pulse can be Gaussian[41] or Fermi-shaped.[19,42] The 2D or 3D UTE sequence is used for acquisition. Using the two source images of the UTE-MT sequence, which includes a regular UTE image without the saturation pulse and one after the saturation pulse, a quantitative off-resonance saturation ratio (OSR) can be derived by subtracting the signal intensity from the two images and dividing by the signal intensity of the UTE image without saturation pulse. This same ratio has also been termed the MT ratio, but OSR is a more correct term because magnetization transfer as well as direct saturation effects are reflected in the ratio.[42–45] Importantly, OSR is highly dependent on the specific technical variables used and varies according to field strength as well as details of the off-resonance saturation pulse (including specific off-resonance frequency and power values).[46]

Applications

Cortical Bone

Osteoporosis is a metabolic bone disease that affects millions of people each year. Insufficiency fractures result in serious long-term disability and death in a large number of patients.[47] About 80% of the skeleton is cortical bone, and ~ 80% of all fractures associated with advanced age arise at sites that are composed of mainly cortical bone.[48] Imaging of bone is important, and dual-energy X-ray absorptiometry (DEXA) represents the most commonly used technique. Unfortunately, measurements of bone mineral density with DEXA only predict fractures with a 30 to 50% success rate.[49–52] The major missing factors in accounting for the risk may be the contribution of bone organic matrix and water to the biomechanical properties of bone. UTE imaging is uniquely suited to address this need, and many qualitative and quantitative UTE techniques were initially developed for use with cortical bone.

Anatomy

Cortical bone is a composite material consisting of mineral (~ 43% by volume), organic matrix (~ 35%), and water (~ 22%).[53,54] Bone mineral provides stiffness and strength; collagen provides ductility and the ability to absorb energy before fracturing. Bone water contributes to viscoelasticity and poroelasticity.[54] Both the material composition and highly complex and hierarchical physical structure contribute to the unique strength of bone.[55]

Water in cortical bone is present at various locations and in different states.[53,54] In normal bone a small fraction of this water exists in a relatively unrestricted (free) form in Haversian canals, with typical diameters > 30 μm, as well as in lacunae and canaliculi, with typical diameters of ~ 10 μm to ~ 0.5 μm, respectively. A larger portion of cortical bone water exists in a restricted (bound) form, either tightly bound to the crystals of the apatite-like mineral or loosely bound to the organic matrix.[56–60] Bound and free water make different contributions to the mechanical properties of bone.[61,62] Bound water is
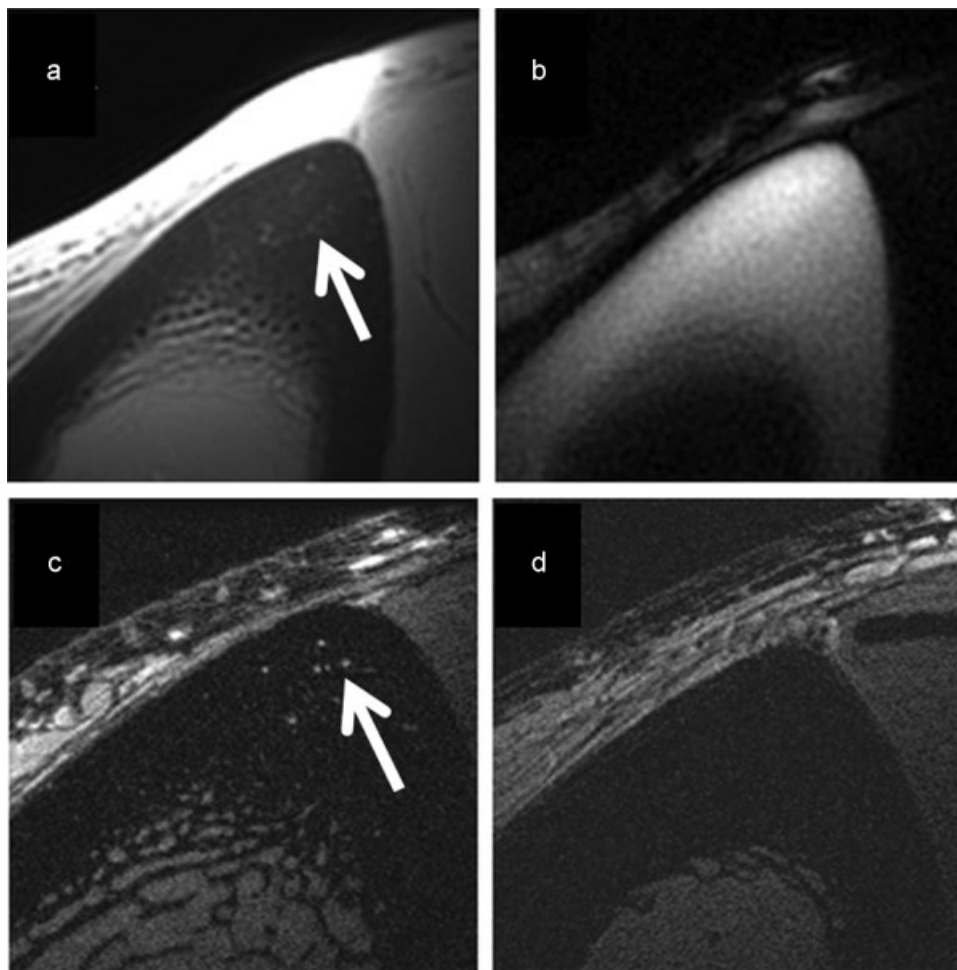
Fig. 4 Axial imaging of the tibia midshaft of a 58-year-old healthy volunteer with (**a**) ultrashort echo time (UTE), (**b**) inversion recovery (IR)-UTE, (**c**) fast spin-echo (FSE) sequences, and (**d**) FSE imaging of the tibia midshaft of a 39-year-old healthy volunteer. UTE detects signal from both bound and free water (a); IR-UTE shows water bound to the organic matrix (b). The fine structures in FSE images (c) correspond to the large Haversian canals, which are more conspicuous compared with the UTE image (arrows). The younger volunteer shows no structure in cortical bone with the FSE sequence, consistent with bone without larger canals (d).
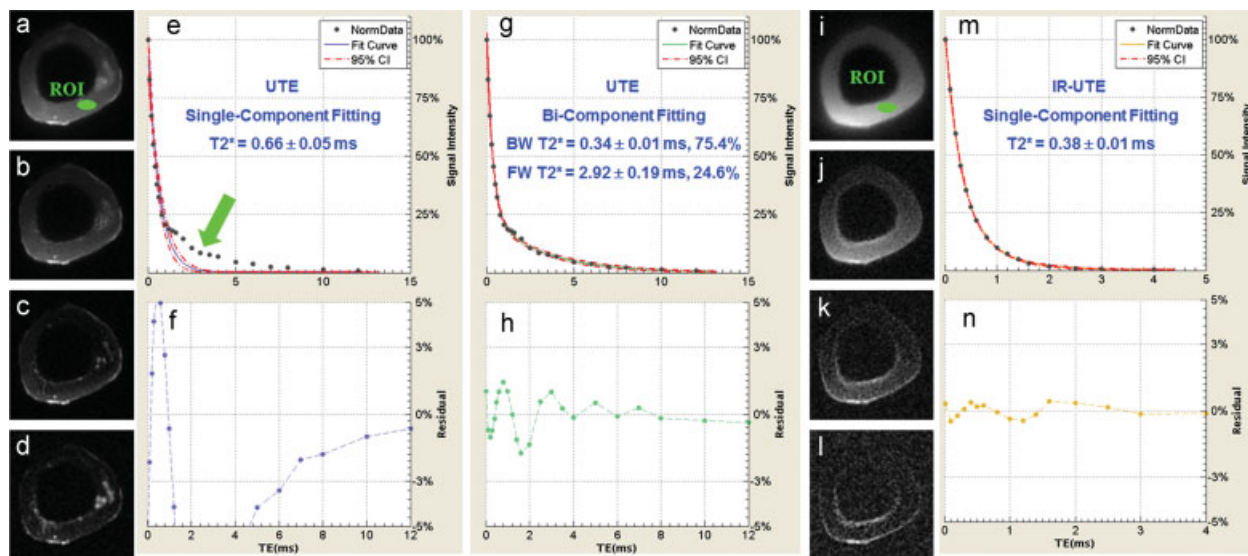
Fig. 5 Selected ultrashort echo time (UTE) images of a human tibia midshaft with TEs of (**a**) 8 µs, (**b**) 0.6 ms, (**c**) 1.6 ms, (**d**) 4 ms, (**e**) single-component, and (**g**) bicomponent fitting as well as signal residues (**f, h**). Selected inversion recovery (IR)-UTE images with TEs of (**i**) 8 µs, (**j**) 0.6 ms, (**k**) 1.2 ms, (**l**) 2.5 ms, (**m**) single-component fitting, and (**n**) residues. The UTE images show both bound and free components; IR-UTE images show only the bound water component. BW, bound water; FW, free water; ROI, region of interest.

directly related to bone strength and toughness, whereas free water is inversely related to modulus of elasticity. Thus it is important to separate the two in studies of bone quality.

Magnetic Resonance Imaging

Using spectroscopic systems, studies have found three pools of protons including collagen methylene protons, collagen-bound water, and a broad peak consisting of pore water and lipid.[61] With UTE sequences, the collagen-bound water and broad peak containing pore water and lipid can be directly detected, but collagen methylene protons cannot because the T2* values are considered supershort (< 50 µs).[63] However,

using MT techniques, all pools may be detected, either directly or indirectly.

Qualitative (►**Fig. 4**) and quantitative UTE techniques have been successfully implemented for the evaluation of the individual pools of water in cortical bone.[18] Single-component T2* values have been reported to be < 1 ms.[39,64] Clinically compatible UTE techniques that can distinguish between bound and free water include T2* with bicomponent analysis, single adiabatic inversion, and double adiabatic inversion[23] (►**Fig. 5**). Recently, two clinically compatible UTE sequence–derived indexes were introduced that significantly correlate with µCT porosity: the porosity index[65,66]
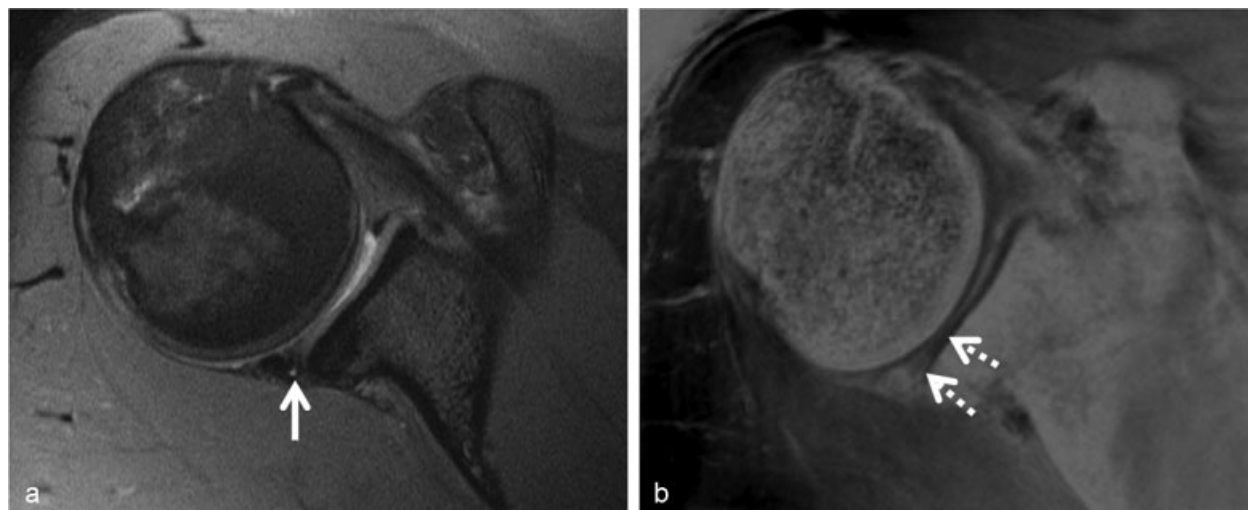
Fig. 6 A 30-year-old professional baseball pitcher. Axial intermediate-weighted fat-suppressed image with (**a**) 23 ms TE and (**b**) three-dimensional ultrashort echo time (3D-UTE)-Cones subtraction image (0.03 ms minus 8.8 ms TEs). Tear of the posterior labrum (arrow) with decentered humeral head is evident on the conventional image. On the subtraction image highlighting short T2 components, there is a relative decrease in short T2 components (water bound to collagen and proteoglycan) within the posterior labrum and posterior third of the glenoid cartilage (dashed arrows). On arthroscopy these regions corresponded to labral degeneration and chondromalacia, respectively. Dual echo-UTE-Cones acquisition time was 4 minutes.

and suppression ratio.[67] The porosity index is calculated from two acquisitions, one with a minimum TE (such as 50 μs), capturing signal from pore water and collagen-bound water, and a second with a longer TE, such as 1.2 ms[65] or 2.0 ms[66] capturing only signal from pore water. The porosity index is defined as the ratio of mean intensity in the longer TE image to that of the minimum TE image. The suppression ratio is also calculated from two acquisitions, one image with long T2* suppression and an unsuppressed image. It is defined as the ratio of mean intensity between the unsuppressed and suppressed images. The concept is that suppression will increase with increasing pore sizes, which are associated with longer T2* values.

Articular Cartilage

Osteoarthritis (OA) is a disease that affects many millions and has a substantial impact on the health care system. Conventional MRI is routinely used for the diagnosis of advanced OA where articular cartilage is significantly damaged or lost. However, conventional MRI is much less sensitive for the detection of OA in the early stages and limited with regard to quantification. Many UTE techniques are well suited for the qualitative and quantitative evaluation of articular cartilage.

Anatomy

Articular hyaline cartilage composition varies by depth from the surface as well as by location in the body. However, it is composed of ∼ 65 to 80% water,[68] and the dry weight is composed of ∼ 60% collagen (predominantly type II) and 12% sulfated proteoglycan.[69,70] Cartilage at weightbearing locations contains more GAG and water compared with nonweightbearing locations.[71–73]

Articular hyaline cartilage demonstrates zonal variability. Four zones have been described including the most superficial zone, tangential zone, middle zone, and deep zone.[74,75] At the superficial regions, collagen fibrils are fine and parallel in orientation with respect to the articular surface. At the deeper regions, collagen fibrils are thicker and perpendicular in orientation with respect to the subchondral bone.[76] In addition, proteoglycan content increases in concentration with increasing depth from the surface.[77] A metabolically active region of calcified cartilage is present at the junction between articular cartilage and subchondral bone, containing type X collagen.[78] This layer of cartilage is ∼ 200 μm in thickness, with decreasing thickness seen with advancing age.[79]

Magnetic Resonance Imaging

Using spectroscopic systems and fresh cartilage plugs obtained from bovine knee joints, studies have found four pools of protons including those associated with collagen (T2 ∼0.02 ms), those associated with mobile proteoglycan (T2 ∼ 1 ms), water molecules trapped within collagen fibrils (T2 ∼ 4 ms), and bulk water (T2 ∼ 20 ms).[80] Conventional MRI techniques with longer TEs capture signal from the abundant bulk water component but are unable to directly visualize any other components.

UTE sequences can be used to detect and highlight the short T2* components (►**Fig. 6**). UTE sequences can also be

used to selectively visualize the calcified layer of cartilage (►**Fig. 2**) that may be involved in the pathogenesis of OA.[81,82] Quantitative T2* analysis obtained with the UTE technique has been shown to be more sensitive to matrix degeneration compared with T2 values obtained with conventional methods.[83] With worsening degeneration, monoexponential UTE-T2* values have been found to decrease.[83] This is an opposite trend compared with conventional T2 values that increase with worsening degeneration. Using bicomponent analysis, a significant correlation between increasing short T2* fractions and worsening degrees of degeneration has been shown.[36]

Menisci of the Knee

The progression of OA is now viewed as a whole-joint process that can result from abnormalities in articular cartilage,
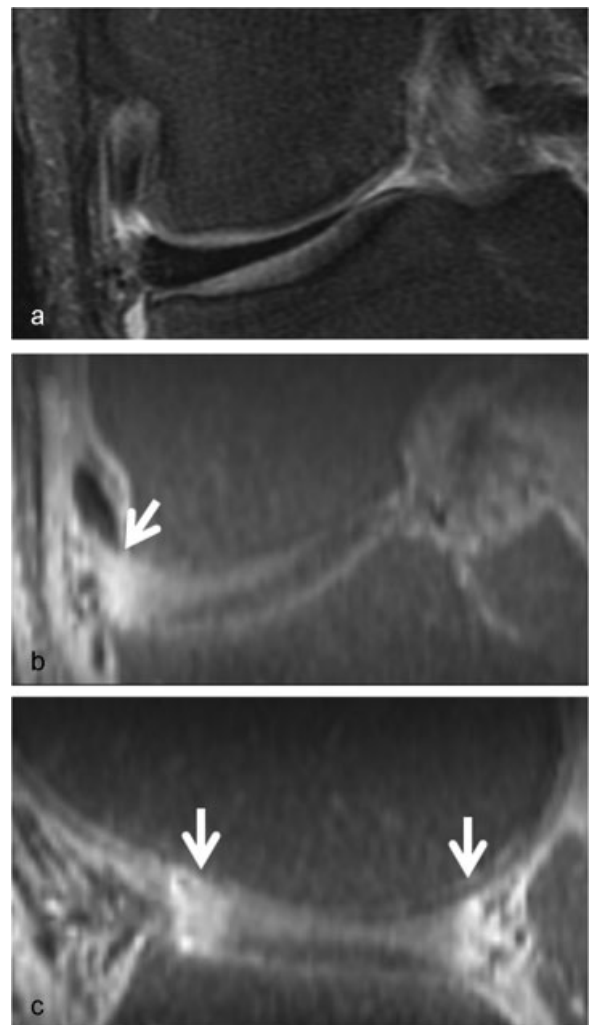
Fig. 7 A 40-year-old man with intact, incomplete discoid lateral meniscus. (**a**) Coronal intermediate-weighted image with 30 ms TE and (**b**) three-dimensional ultrashort echo time (3D UTE)-Cones subtraction images (0.03 ms minus 12 ms TEs) of the lateral meniscus 90 minutes after intravenous gadolinium contrast administration, reformatted into (**b**) coronal and (**c**) sagittal planes. On the conventional image, there is no signal within the meniscus and no opportunity to visualize contrast enhancement. In comparison, UTE subtraction images demonstrate abundant signal and visualization of contrast, which has diffused into the peripheral 3 to 4 mm of meniscus (arrows). Dual echo-UTE-Cones acquisition time was ∼ 2.5 minutes.

subchondral bone, synovium, capsule, and meniscus.[84] Located between the femoral condyles and tibial plateaus, the menisci play important roles in load transmission, shock absorption, and maintenance of joint stability.[85] Mechanical impairment of the meniscus alters the weightbearing capacities of the knee joint, leading to damage to the adjacent articular cartilage and subchondral bone, eventually contributing to the progression of OA.[86,87] Menisci are predominantly hypointense on conventional imaging, which reflects the predominance of short T2/T2* components. UTE imaging is well suited for the qualitative and quantitative evaluation of meniscal tissue.

Anatomy

The menisci of the knee are composed of $\sim$ 70% water, and the dry weight is composed of $\sim$ 60 to 70% collagen and 2 to 8% proteoglycan.[88] The hierarchical fiber structure of the knee menisci is complex, with circumferential bundles representing the largest group.[89,90] Radial fibers are another prominent fiber group and can appear as large bundles, referred to as radial ties or sheets.[91] Similar to cartilage, meniscal composition also shows zonal heterogeneity, with the peripheral portion containing higher vascularity[92] and a smaller concentration of proteoglycan.[93]

Magnetic Resonance Imaging

UTE imaging has been used to demonstrate the fibrocartilage and fibrillary network of the menisci.[94] After intravenous contrast administration with UTE acquisition, the vascularized portions of the meniscus and meniscal root ligaments can be readily visualized[95] (►Fig. 7). Meniscal calcifications are also readily identified and can be quantified using UTE imaging.[96] Quantitative UTE imaging with monoexponential T2* analysis has been used to demonstrate subclinical meniscus degeneration.[97] With bicomponent T2* analysis, quantification of normal versus abnormal meniscal regions can be made.[4,31] Changes in meniscal proteoglycan and GAG content can be detected with the UTE-T1ρ sequence.[37]

Spine (Intervertebral Disks)

Low back pain is a debilitating condition. Although multifactorial, intervertebral disk (IVD) degeneration is one cause of chronic back pain,[98,99] and disk degeneration can lead to disk
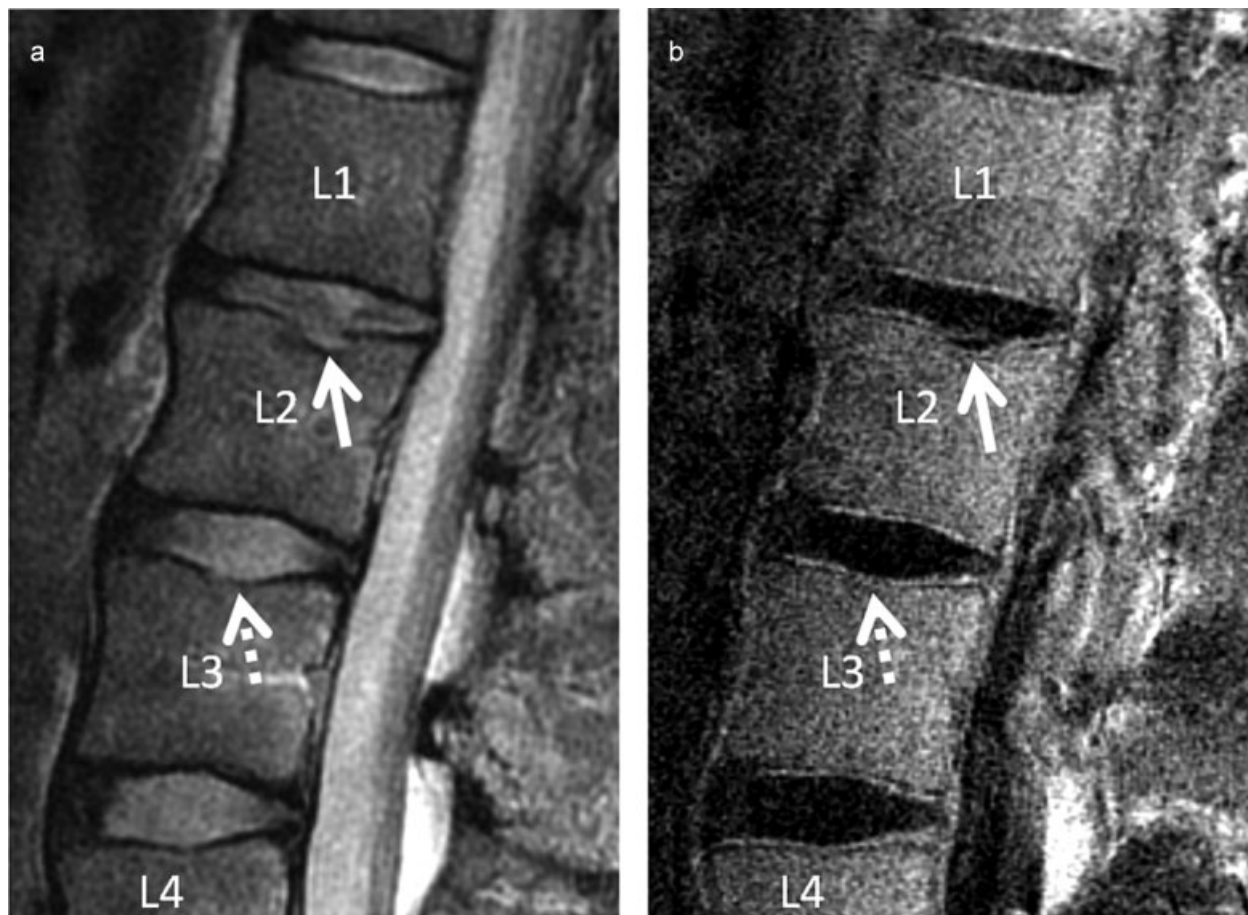
Fig. 8 Sagittal images of the lumbar spine using T2-weighted fast spin-echo (FSE) with TE 87 ms (a) and three-dimensional ultrashort echo time (3D-UTE)-Cones subtraction technique (0.03 ms minus 4.6 ms TEs) (b). Notice the herniated nucleus pulposus through the superior end plates of L2 and L3 (Schmorl nodes), with corresponding depression (arrow) and disruption (dashed arrow) of hyperintense lines on the subtraction image, representing altered calcified cartilaginous end plates (CEPs). The nucleus pulposi at these affected levels are more desiccated compared with T12–L1 and L3–L4, where the CEPs were intact. Dual-echo-UTE-Cones acquisition time was $\sim$ 5 minutes.

herniation and radicular pain. Although the exact pathogenesis is unknown, disk degeneration may involve alterations in tissues of the diskovertebral junction (DVJ), which provides mechanical and nutritional support. Conventional MR imaging of the lumbar spine has focused on morphological evaluation of the disk. UTE techniques enable imaging of the DVJ with high contrast, as well as new ways of evaluating the disk proper.

Anatomy

The human spine comprises 23 IVDs positioned between vertebrae that facilitate back movement. The IVDs are bounded peripherally by the anterior and posterior longitudinal ligaments of the spine and axially by the cartilaginous end plates[100] at the DVJ. The IVDs consist of a gelatinous nucleus pulposus (NP) in the center, surrounded by annulus fibrosus (AF). Healthy NPs are well hydrated (70–90% water) and rich in GAGs (65% of dry weight). The AF has markedly less water content (60–70%) and is rich in collagen (50–60% of dry weight) that form concentric lamellae that alternate in orientation.[101,102]

At the DVJ, cartilaginous end plates (CEPs) form an interface between the IVD proper and vertebral body. The CEP in adults consists of layers of uncalcified and calcified cartilage[103] that is ~ 1 mm thick.[104] The vertebral body provides a bed of capillaries that adhere directly onto the CEP, providing metabolites needed for the cell of the IVD.

Magnetic Resonance Imaging

The IVD is generally considered a tissue with fairly long T2 values ranging from ~ 40 ms in the AF to > 80 ms in the NP. Conventional MR imaging typically utilizes fast spin-echo sequences in the sagittal plane, with long TEs up to 100 ms that are capable of revealing the morphologic characteristics of the NP.[105] However, the region of the DVJ is seen with low signal intensity with conventional imaging (►Fig. 8a). This makes it difficult for morphological evaluation and impossible for quantitative analysis. Using UTE techniques, the region of the DVJ is seen with great contrast in vivo (►Fig. 8b). The CEP is seen as a continuous, linear, and high signal intensity line in normal cases; regions with the Schmorl node formation and bony end-plate irregularity exhibit loss of the normal characteristics (►Fig. 8b).

Conclusion

Ultrashort TE sequences provide a method to image tissues and tissue components that have not previously been visible using conventional clinical sequences. Continuing modifications to this technique have allowed for faster and more robust sequences that allow for morphological imaging and quantitative evaluation of short T2/T2* tissues in vivo. The combination of vendor incorporation of UTE sequences into their update packages and continuing validation from research studies will lead to increasing acceptance and utilization by musculoskeletal radiologists.

References

1 Bydder GM. Review. The Agfa Mayneord lecture: MRI of short and ultrashort T$_2$ and T$_2$ components of tissues, fluids and materials using clinical systems. Br J Radiol 2011;84(1008):1067–1082

2 Geva T. Magnetic resonance imaging: historical perspective. J Cardiovasc Magn Reson 2006;8(4):573–580

3 Smith FW. Clinical application of NMR tomographic imaging. In: Witcofski RL, Karstaedt N, Partain CL, eds. NMR imaging. Winston Salem, NC: Bowman Gray School of Medicine; 1982:125–132

4 Chang EY, Du J, Chung CB. UTE imaging in the musculoskeletal system. J Magn Reson Imaging 2015;41(4):870–883

5 Pauly JM, Conolly SI, Nishimura D, et al. Slice-selective excitation for very short T2 species. Paper presented at: ISMRM 8th Scientific Meeting and Exhibition; 1989; Amsterdam, Netherlands

6 Rahmer J, Börnert P, Groen J, Bos C. Three-dimensional radial ultrashort echo-time imaging with T2 adapted sampling. Magn Reson Med 2006;55(5):1075–1082

7 Robson MD, Gatehouse PD, Bydder M, Bydder GM. Magnetic resonance: an introduction to ultrashort TE (UTE) imaging. J Comput Assist Tomogr 2003;27(6):825–846

8 Du J, Bydder M, Takahashi AM, Chung CB. Two-dimensional ultrashort echo time imaging using a spiral trajectory. Magn Reson Imaging 2008;26(3):304–312

9 Gurney PT, Hargreaves BA, Nishimura DG. Design and analysis of a practical 3D cones trajectory. Magn Reson Med 2006;55(3):575–582

10 Qian Y, Boada FE. Acquisition-weighted stack of spirals for fast high-resolution three-dimensional ultra-short echo time MR imaging. Magn Reson Med 2008;60(1):135–145

11 Song HK, Wehrli FW. Variable TE gradient and spin echo sequences for in vivo MR microscopy of short T2 species. Magn Reson Med 1998;39(2):251–258

12 Weiger M, Pruessmann KP. MRI with zero echo time. In: eMagRes. John Wiley & Sons; 2012. Abstract available at:http://onlinelibrary.wiley.com/doi/10.1002/9780470034590.emrstm1292/abstract. Accessed September 2, 2015

13 Wiesinger F, Sacolick LI, Menini A, et al. Zero TE MR bone imaging in the head. Magn Reson Med 2015; January 16 (Epub ahead of print)

14 Garwood M, Idiyatullin D, Corum CA, et al. Capturing signals from fast-relaxing spins with frequency-swept MRI: SWIFT. In: eMagRes. John Wiley & Sons; 2012. Abstract available at: http://onlinelibrary.wiley.com/doi/10.1002/9780470034590.emrstm1259/abstract. Accessed September 2, 2015

15 Grodzki DM, Jakob PM, Heismann B. Ultrashort echo time imaging using pointwise encoding time reduction with radial acquisition (PETRA). Magn Reson Med 2012;67(2):510–518

16 Lee YH, Kim S, Song HT, Kim I, Suh JS. Weighted subtraction in 3D ultrashort echo time (UTE) imaging for visualization of short T2 tissues of the knee. Acta Radiol 2014;55(4):454–461

17 Wu Y, Ackerman JL, Chesler DA, Graham L, Wang Y, Glimcher MJ. Density of organic matrix of native mineralized bone measured by water- and fat-suppressed proton projection MRI. Magn Reson Med 2003;50(1):59–68

18 Du J, Bydder GM. Qualitative and quantitative ultrashort-TE MRI of cortical bone. NMR Biomed 2013;26(5):489–506

19 Du J, Takahashi AM, Bydder M, Chung CB, Bydder GM. Ultrashort TE imaging with off-resonance saturation contrast (UTE-OSC). Magn Reson Med 2009;62(2):527–531

20 Henkelman RM, Stanisz GJ, Graham SJ. Magnetization transfer in MRI: a review. NMR Biomed 2001;14(2):57–64

21 Maryanski MJ, Gore JC, Kennan RP, Schulz RJ. NMR relaxation enhancement in gels polymerized and cross-linked by ionizing radiation: a new approach to 3D dosimetry by MRI. Magn Reson Imaging 1993;11(2):253–258

22 Ward KM, Aletras AH, Balaban RS. A new class of contrast agents for MRI based on proton chemical exchange dependent saturation transfer (CEST). J Magn Reson 2000;143(1):79–87

23 Horch RA, Gochberg DF, Nyman JS, Does MD. Clinically compatible MRI strategies for discriminating bound and pore water in cortical bone. Magn Reson Med 2012;68(6):1774–1784

24 Reichert IL, Robson MD, Gatehouse PD, et al. Magnetic resonance imaging of cortical bone with ultrashort TE pulse sequences. Magn Reson Imaging 2005;23(5):611–618

25 Du J, Carl M, Bae WC, et al. Dual inversion recovery ultrashort echo time (DIR-UTE) imaging and quantification of the zone of calcified cartilage (ZCC). Osteoarthritis Cartilage 2013;21(1):77–85

26 Du J, Takahashi AM, Bae WC, Chung CB, Bydder GM. Dual inversion recovery, ultrashort echo time (DIR UTE) imaging: creating high contrast for short-T(2) species. Magn Reson Med 2010;63(2):447–455

27 Carl M, Chiang J-TA. Investigations of the origin of phase differences seen with ultrashort TE imaging of short T2 meniscal tissue. Magn Reson Med 2012;67(4):991–1003

28 Haacke EM, Xu Y, Cheng YC, Reichenbach JR. Susceptibility weighted imaging (SWI). Magn Reson Med 2004;52(3):612–618

29 Gore JC, Anderson AW. The physics of relaxation. In: eMagRes. John Wiley & Sons; 2013. Abstract available at: http://onlinelibrary.wiley.com/doi/10.1002/9780470034590.emrstm1282/abstract. Accessed September 2, 2015

30 Bergin CJ, Pauly JM, Macovski A. Lung parenchyma: projection reconstruction MR imaging. Radiology 1991;179(3):777–781

31 Du J, Diaz E, Carl M, Bae W, Chung CB, Bydder GM. Ultrashort echo time imaging with bicomponent analysis. Magn Reson Med 2012;67(3):645–649

32 Xia Y. MRI of articular cartilage at microscopic resolution. Bone Joint Res 2013;2(1):9–17

33 Chang EY, Du J, Iwasaki K, et al. Single- and Bi-component T2* analysis of tendon before and during tensile loading, using UTE sequences. J Magn Reson Imaging 2015;42(1):114–120

34 Fullerton GD, Cameron IL, Ord VA. Orientation of tendons in the magnetic field and its effect on T2 relaxation times. Radiology 1985;155(2):433–435

35 Wang N, Xia Y. Anisotropic analysis of multi-component T2 and T1rho relaxations in achilles tendon by NMR spectroscopy and microscopic MRI. J Magn Reson Imaging 2013;38(3):625–633

36 Pauli C, Bae WC, Lee M, et al. Ultrashort-echo time MR imaging of the patella with bicomponent analysis: correlation with histopathologic and polarized light microscopic findings. Radiology 2012;264(2):484–493

37 Du J, Carl M, Diaz E, et al. Ultrashort TE T1rho (UTE T1rho) imaging of the Achilles tendon and meniscus. Magn Reson Med 2010;64(3):834–842

38 Du J, Statum S, Znamirowski R, Bydder GM, Chung CB. Ultrashort TE T1ρ magic angle imaging. Magn Reson Med 2013;69(3):682–687

39 Du J, Carl M, Bydder M, Takahashi A, Chung CB, Bydder GM. Qualitative and quantitative ultrashort echo time (UTE) imaging of cortical bone. J Magn Reson 2010;207(2):304–311

40 Springer F, Steidle G, Martirosian P, Syha R, Claussen CD, Schick F. Rapid assessment of longitudinal relaxation time in materials and tissues with extremely fast signal decay using UTE sequences and the variable flip angle method. Invest Radiol 2011;46(10):610–617

41 Springer F, Martirosian P, Machann J, Schwenzer NF, Claussen CD, Schick F. Magnetization transfer contrast imaging in bovine and human cortical bone applying an ultrashort echo time sequence at 3 Tesla. Magn Reson Med 2009;61(5):1040–1048

42 Syha R, Martirosian P, Ketelsen D, et al. Magnetization transfer in human Achilles tendon assessed by a 3D ultrashort echo time sequence: quantitative examinations in healthy volunteers at 3T. Rofo 2011;183(11):1043–1050

43 Grosse U, Syha R, Martirosian P, et al. Ultrashort echo time MR imaging with off-resonance saturation for characterization of pathologically altered Achilles tendons at 3 T. Magn Reson Med 2013;70(1):184–192

44 Hodgson RJ, Grainger AJ, O'Connor PJ, et al. Imaging of the Achilles tendon in spondyloarthritis: a comparison of ultrasound and conventional, short and ultrashort echo time MRI with and without intravenous contrast. Eur Radiol 2011;21(6):1144–1152

45 Chang EY, Du J, Biswas R, et al. Off-resonance saturation ratio obtained with ultrashort echo time-magnetization transfer techniques is sensitive to changes in static tensile loading of tendons and degeneration. J Magn Reson Imaging 2015; March 23 (Epub ahead of print)

46 Stanisz GJ, Odrobina EE, Pun J, et al. T1, T2 relaxation and magnetization transfer in tissue at 3T. Magn Reson Med 2005;54(3):507–512

47 [No authors listed]. NIH Consensus Development Panel on Osteoporosis Prevention, Diagnosis, and Therapy, March 7–29, 2000: highlights of the conference. South Med J 2001;94(6):569–573

48 Zebaze RMD, Ghasem-Zadeh A, Bohte A, et al. Intracortical remodelling and porosity in the distal radius and post-mortem femurs of women: a cross-sectional study. Lancet 2010;375(9727):1729–1736

49 Marshall D, Johnell O, Wedel H. Meta-analysis of how well measures of bone mineral density predict occurrence of osteoporotic fractures. BMJ 1996;312(7041):1254–1259

50 Schuit SCE, van der Klift M, Weel AE, et al. Fracture incidence and association with bone mineral density in elderly men and women: The Rotterdam Study. Bone 2004;34(1):195–202

51 McCreadie BR, Goldstein SA. Biomechanics of fracture: is bone mineral density sufficient to assess risk? J Bone Miner Res 2000;15(12):2305–2308

52 Homminga J, McCreadie BR, Ciarelli TE, Weinans H, Goldstein SA, Huiskes R. Cancellous bone mechanical properties from normals and patients with hip fractures differ on the structure level, not on the bone hard tissue level. Bone 2002;30(5):759–764

53 Cowin SC. Bone poroelasticity. J Biomech 1999;32(3):217–238

54 Wehrli FW, Song HK, Saha PK, Wright AC. Quantitative MRI for the assessment of bone structure and function. NMR Biomed 2006;19(7):731–764

55 Ritchie RO, Buehler MJ, Hansma P. Plasticity and toughness in bone. Physics Today 2009;62:41–47. Available at: http://web.mit.edu/mbuehler/www/research/PTO000041.pdf

56 Wang X, Ni Q. Determination of cortical bone porosity and pore size distribution using a low field pulsed NMR approach. J Orthop Res 2003;21(2):312–319

57 Nyman JS, Ni Q, Nicolella DP, Wang X. Measurements of mobile and bound water by nuclear magnetic resonance correlate with mechanical properties of bone. Bone 2008;42(1):193–199

58 Horch RA, Nyman JS, Gochberg DF, Dortch RD, Does MD. Characterization of 1H NMR signal in human cortical bone for magnetic resonance imaging. Magn Reson Med 2010;64(3):680–687

59 Diaz E, Chung CB, Bae WC, et al. Ultrashort echo time spectroscopic imaging (UTESI): an efficient method for quantifying bound and free water. NMR Biomed 2012;25(1):161–168

60 Biswas R, Bae W, Diaz E, et al. Ultrashort echo time (UTE) imaging with bi-component analysis: bound and free water evaluation of bovine cortical bone subject to sequential drying. Bone 2012; 50(3):749–755

61 Horch RA, Gochberg DF, Nyman JS, Does MD. Non-invasive predictors of human cortical bone mechanical properties: T(2)-discriminated H NMR compared with high resolution X-ray. PLoS ONE 2011;6(1):e16359

62 Bae WC, Chen PC, Chung CB, Masuda K, D'Lima D, Du J. Quantitative ultrashort echo time (UTE) MRI of human cortical bone: correlation with porosity and biomechanical properties. J Bone Miner Res 2012;27(4):848–857

63 Fernández-Seara MA, Wehrli SL, Takahashi M, Wehrli FW. Water content measured by proton-deuteron exchange NMR predicts bone mineral density and mechanical properties. J Bone Miner Res 2004;19(2):289–296

64 Techawiboonwong A, Song HK, Leonard MB, Wehrli FW. Cortical bone water: in vivo quantification with ultrashort echo-time MR imaging. Radiology 2008;248(3):824–833

65 Bashoor-Zadeh M, Li C, Sun W, et al. Simple ultrashort echo time MRI measure associated with cortical bone porosity. Paper presented at: ISMRM 21th Scientific Meeting & Exhibition; 2013; Salt Lake City, UT

66 Rajapakse CS, Bashoor-Zadeh M, Li C, Sun W, Wright AC, Wehrli FW. Volumetric cortical bone porosity assessment with MR imaging: validation and clinical feasibility. Radiology 2015; 276(2):526–535

67 Li C, Seifert AC, Rad HS, et al. Cortical bone water concentration: dependence of MR imaging measures on age and pore volume fraction. Radiology 2014;272(3):796–806

68 Maroudas A. Physico-chemical properties of articular cartilage. In: Freeman MAR, ed. Adult Articular Cartilage. 2nd ed. Tunbridge Wells, UK: Pitman Medical; 1979:215–290

69 Sophia Fox AJ, Bedi A, Rodeo SA. The basic science of articular cartilage: structure, composition, and function. Sports Health 2009;1(6):461–468

70 Johnson D, Pedowitz RA. Practical Orthopaedic Sports Medicine and Arthroscopy. Philadelphia, PA: Lippincott Williams & Wilkins; 2007

71 Rogers BA, Murphy CL, Cannon SR, Briggs TW. Topographical variation in glycosaminoglycan content in human articular cartilage. J Bone Joint Surg Br 2006;88(12):1670–1674

72 Rogers B, Murphy C, Cannon S, et al. P100 topographical glycosaminoglycan variation in human articular cartilage. J Bone Joint Surg Br 2008;90-B(II):391

73 Yoshida K, Azuma H. Contents and compositions of glycosaminoglycans in different sites of the human hip joint cartilage. Ann Rheum Dis 1982;41(5):512–519

74 Hunziker EB, Michel M, Studer D. Ultrastructure of adult human articular cartilage matrix after cryotechnical processing. Microsc Res Tech 1997;37(4):271–284

75 Fujioka R, Aoyama T, Takakuwa T. The layered structure of the articular surface. Osteoarthritis Cartilage 2013;21(8): 1092–1098

76 Aspden RM, Hukins DW. Collagen organization in articular cartilage, determined by X-ray diffraction, and its relationship to tissue function. Proc R Soc Lond B Biol Sci 1981;212(1188): 299–304

77 Muir H. Proteoglycans of cartilage. J Clin Pathol Suppl (R Coll Pathol) 1978;12:67–81

78 Schmid TM, Linsenmayer TF. Immunohistochemical localization of short chain cartilage collagen (type X) in avian tissues. J Cell Biol 1985;100(2):598–605

79 Lane LB, Bullough PG. Age-related changes in the thickness of the calcified zone and the number of tidemarks in adult human articular cartilage. J Bone Joint Surg Br 1980;62(3): 372–375

80 Lattanzio PJ, Marshall KW, Damyanovich AZ, Peemoeller H. Macromolecule and water magnetization exchange modeling in articular cartilage. Magn Reson Med 2000;44(6): 840–851

81 Boyde A, Riggs CM, Bushby AJ, McDermott B, Pinchbeck GL, Clegg PD. Cartilage damage involving extrusion of mineralisable matrix from the articular calcified cartilage and subchondral bone. Eur Cell Mater 2011;21:470–478; discussion 478

82 Bae WC, Dwek JR, Znamirowski R, et al. Ultrashort echo time MR imaging of osteochondral junction of the knee at 3 T: identification of anatomic structures contributing to signal intensity. Radiology 2010;254(3):837–845

83 Williams A, Qian Y, Bear D, Chu CR. Assessing degeneration of human articular cartilage with ultra-short echo time (UTE) T2* mapping. Osteoarthritis Cartilage 2010;18(4):539–546

84 Brandt KD, Radin EL, Dieppe PA, van de Putte L. Yet more evidence that osteoarthritis is not a cartilage disease. Ann Rheum Dis 2006; 65(10):1261–1264

85 Fukubayashi T, Kurosawa H. The contact area and pressure distribution pattern of the knee. A study of normal and osteoarthrotic knee joints. Acta Orthop Scand 1980;51(6):871–879

86 Berthiaume MJ, Raynauld JP, Martel-Pelletier J, et al. Meniscal tear and extrusion are strongly associated with progression of symptomatic knee osteoarthritis as assessed by quantitative magnetic resonance imaging. Ann Rheum Dis 2005;64(4): 556–563

87 Sharma L, Eckstein F, Song J, et al. Relationship of meniscal damage, meniscal extrusion, malalignment, and joint laxity to subsequent cartilage loss in osteoarthritic knees. Arthritis Rheum 2008;58(6):1716–1726

88 Blain E, Duance V. Meniscus. In: Hutson MA, Speed C, eds. Sports Injuries. Oxford, UK, and New York, NY: Oxford University Press; 2011:45–53

89 Petersen W, Tillmann B. Collagenous fibril texture of the human knee joint menisci. Anat Embryol (Berl) 1998;197(4): 317–324

90 Kambic HE, McDevitt CA. Spatial organization of types I and II collagen in the canine meniscus. J Orthop Res 2005;23(1): 142–149

91 Skaggs DL, Warden WH, Mow VC. Radial tie fibers influence the tensile properties of the bovine medial meniscus. J Orthop Res 1994;12(2):176–185

92 Arnoczky SP, Warren RF. Microvasculature of the human meniscus. Am J Sports Med 1982;10(2):90–95

93 Nakano T, Dodd CM, Scott PG. Glycosaminoglycans and proteoglycans from different zones of the porcine knee meniscus. J Orthop Res 1997;15(2):213–220

94 Bae WC, Du J, Bydder GM, Chung CB. Conventional and ultrashort time-to-echo magnetic resonance imaging of articular cartilage, meniscus, and intervertebral disk. Top Magn Reson Imaging 2010;21(5):275–289

95 Gatehouse PD, He T, Puri BK, Thomas RD, Resnick D, Bydder GM. Contrast-enhanced MRI of the menisci of the knee using ultrashort echo time (UTE) pulse sequences: imaging of the red and white zones. Br J Radiol 2004;77(920):641–647

96 Omoumi P, Bae WC, Du J, et al. Meniscal calcifications: morphologic and quantitative evaluation by using 2D inversion-recovery ultrashort echo time and 3D ultrashort echo time 3.0-T MR imaging techniques—feasibility study. Radiology 2012;264(1): 260–268

97 Williams A, Qian Y, Golla S, Chu CR. UTE-T2* mapping detects subclinical meniscus injury after anterior cruciate ligament tear. Osteoarthritis Cartilage 2012;20(6):486–494

98 Andersson GB. Epidemiological features of chronic low-back pain. Lancet 1999;354(9178):581–585

99 An HS, Anderson PA, Haughton VM, et al. Introduction: disc degeneration: summary. Spine 2004;29(23):2677–2678

100 Bogduk N, Endres SM. Clinical Anatomy of the Lumbar Spine and Sacrum. 4th ed. New York, NY: Elsevier/Churchill Livingstone; 2005

101 Marchand F, Ahmed AM. Investigation of the laminate structure of lumbar disc anulus fibrosus. Spine 1990;15(5):402–410

102 Cassidy JJ, Hiltner A, Baer E. Hierarchical structure of the intervertebral disc. Connect Tissue Res 1989;23(1):75–88

103 Setton LA, Zhu W, Weidenbaum M, Ratcliffe A, Mow VC. Compressive properties of the cartilaginous end-plate of the baboon lumbar spine. J Orthop Res 1993;11(2): 228–239

104 Roberts S, Menage J, Urban JP. Biochemical and structural properties of the cartilage end-plate and its relation to the intervertebral disc. Spine 1989;14(2):166–174

105 Pfirrmann CW, Metzdorf A, Zanetti M, Hodler J, Boos N. Magnetic resonance classification of lumbar intervertebral disc degeneration. Spine 2001;26(17):1873–1878